



Large Deformation Failure Characteristics and Control Measures for Squeezing Tunnels with Steeply Inclined and Layered Rock in Strong and Active Fault Zones: A Case Study

Songtao Li^{1,2} · Zhongsheng Tan² · Yujie Wang¹ · Yang Yang^{2,3}

Received: 10 October 2023 / Revised: 20 January 2024 / Accepted: 17 February 2024 / Published online: 18 May 2024
© The Author(s), under exclusive licence to the Iran University of Science and Technology 2024

Abstract

The complex mechanical behaviours of steeply inclined and layered surrounding rock in strong and active fault zones result in control measures that cannot adapt to asymmetric squeezing tunnel and are still unsolved. Hence, the Yuntunbao Tunnel was taken as an example to study this issue based on geological survey and indoor and outdoor tests. The results showed that strong geological structures and abundant groundwater undoubtedly deteriorate the mechanical properties of rocks containing many water-sensitive minerals, approximately 45%. The stepwise growth of deformation characteristics before reaching the rock peak strength and the gradient to abrupt failure characteristics after reaching the rock peak strength are determined via triaxial cyclic and static load tests. According to field test results, the unilateral squeezing deformation is severe and greater than 1.5 m, the average extent of the excavation loosening zone is approximately 10 m, and the highest deformation rate reaches 12 cm/d. The gradual and sudden changes in tunnel deformation are demonstrated to be consistent with the postpeak deformation characteristics of layered rock in indoor tests. Moreover, the steel arch exhibits composite failure characteristics of bending and torsion. Finally, reliable and practical controlling measures are suggested, including the optimised three-bench excavation method with reserved core soil, advanced parallel pilot tunnel, long and short rock bolts, and large lock-foot anchor pipe. Compared with tunnel deformation before taking measures, the maximum convergence deformation is reduced from 2.7 to 0.9 m, and the bearing force of the primary support is also reasonable and stable.

Keywords Inclined and layered rock · Deformation failure characteristics · Squeezing effect · Cyclic loading and unloading · Deformation control measures

1 Introduction

The complex and changeable geological environment in Western China has brought significant challenges to large-scale underground engineering construction [1–4]. These underground projects were constructed in areas with strong

tectonic action. Therefore, they are bound to encounter a series of technical engineering problems, such as water and mud gushing in the fault fracture zone, rock bursts, and large deformations. Amongst them, large deformation tunnels are amongst the most complicated and are accompanied by severe steel arch bending and breaking, large area spalling of shotcrete, tunnel lining cracking and

✉ Songtao Li
list@iwhr.com
Zhongsheng Tan
zhsthan@bjtu.edu.cn
Yujie Wang
wangyj@iwhr.com
Yang Yang
youngyang_dec@163.com

¹ China State Key Laboratory of Simulation and Regulation of Water Cycle in River Basin, China Institute of Water Resources and Hydropower Research, Beijing 100044, China
² Key Laboratory of Urban Underground Engineering, Ministry of Education, Beijing Jiaotong University, Beijing 100044, China
³ China Railway Economic and Planning Research Institute, Beijing 100044, China

tunnel face collapse [5–9]. In particular, tunnelling through layered strata easily causes asymmetric deformation and failure responses of support structures [10–14].

The anisotropic mechanical properties of layered rock significantly affected by weak planes have long been recognised [15, 16]. Considerable research has been undertaken to study the mechanical behaviour of phyllite, slate and shale specimens, such as failure characteristics, strength criteria and bedding planes, under uniaxial and triaxial stress states [17–21]. However, these studies have mainly concentrated on static loads, but recent studies have shown that the fatigue damage and deformation failure of rock under cyclic loads require increased attention [22–24]. The deformation characteristics, failure modes, mechanical parameters and irreversible strain of the layered rock were evaluated via multistage triaxial cyclic load tests [25]. To explore the mechanical behaviour of sandstone specimens with prefabricated cracks, true triaxial cyclic loading and unloading tests were also implemented [26]. In addition, similar materials were used to make layered rock samples. Given the deformation and failure of artificial layered materials with different inclination angles, the smaller the inclination angle of the structural plane of the sample is, the greater the ageing deformation and creep rate are [27].

Based on this brief literature survey, the mechanical response and failure modes of layered rocks under different stress states are substantially different. However, from an engineering perspective, the intensity and amplitude of the disturbed stress in the surrounding rock change dynamically and are not continuous during tunnelling [28, 29]. Therefore, the load characteristics of rock are not simply subjected to triaxial cyclic loading and unloading; the creep effect also occurs. Presently, studies on the mechanical properties of structural plane rock in response to dynamic loads in the creep state are rare.

Furthermore, because of the unique mechanical properties and deformation behaviour of layered and soft rock, many studies have investigated the control of large squeezing deformation tunnels. These include the stress release of the pilot tunnel [30], tunnel cross-sectional optimization [31], closure distance of the primary support [32], tunnel lining with a yielding layer [33], construction time of the tunnel lining [34] and multilayer primary support structure [35–37]. Moreover, considering the large deformation amount and long-duration deformation characteristics, yielding structures are also applied to control the surrounding rock deformation. For example, a retractable arch [38], compressible concrete members [39] and a primary structural damper have been adopted [40]. Unlike “passive” controlling deformation components, the timely application of anchor bolts, especially prestressed anchor bolts, also effectively improves the bearing capacity of the surrounding rock [41–43]. However, for layered and broken surrounding

rock, prestressed bolts still have several problems associated with prestress, shear bending and dislocation of rock bolts.

Overall, the deformation failure mechanism of layered rock under cyclic loads remains poorly understood. More attention has been given to the loading rate, stress state and disturbance stress threshold. For squeezing tunnel engineering, the creep behaviour of the surrounding rock is a main factor that leads to support structure failure. However, few studies have comprehensively considered the creep effect and periodic loads on the deformation failure of layered rock. In addition, for large squeezing tunnels with inclined layered strata in strong and active tectonic regions, preventing structural instability of double primary supports and controlling uncoordinated settlement deformation have not been performed. Therefore, this paper describes the use of a typical large squeezing deformation tunnel to study and resolve this issue via geological investigation and laboratory and field tests. The research results can provide a reliable reference for subsequent similar projects.

2 Project Overview

2.1 Strong Regional Tectonism

Relying on the critical engineering of the Chengdu Lanzhou Railway-Yuntunpu Tunnel, the total tunnel length is 22.92 km, and the maximum burial depth of the tunnel is approximately 750 m. The tunnel site is located in the Minshan uplift fault block, which is located at the eastern margin of the Tibetan Plateau [44, 45], as shown in Fig. 1.

The eastern, western, southern and northern boundaries of the Minshan fault block are the Huya, Minjiang, Maowen and Tazang faults, respectively. Moreover, geological tectonic activity around fault blocks is frequent [46]. Global Positioning System (GPS) data show that the Minshan fault block is highly active, with an overall motion rate exceeding 2 mm/a [47]. The length of the Minjiang fault is approximately 180 km, and the fault strikes nearly N–S and dips NW, with a dip angle of 40°–70°. The layout of the tunnel line is strongly affected by the Minjiang fault (Fig. 2). The horizontal principal stress is the main stress in this region, and the maximum measured principal stress is more than 15 MPa. In addition, many secondary folds exist around the tunnel site (Fig. 3). Therefore, in the initial state, a very high squeezing deformation energy is stored inside the rock mass, the mechanical properties of the rock mass are very poor, and the stress state of the surrounding rock is also strongly affected during tunnelling.

2.2 Tunnel Cross-section and Support Structures

The tunnel is a single-hole double-line tunnel with a span of approximately 16 m and a height of approximately 15 m, and

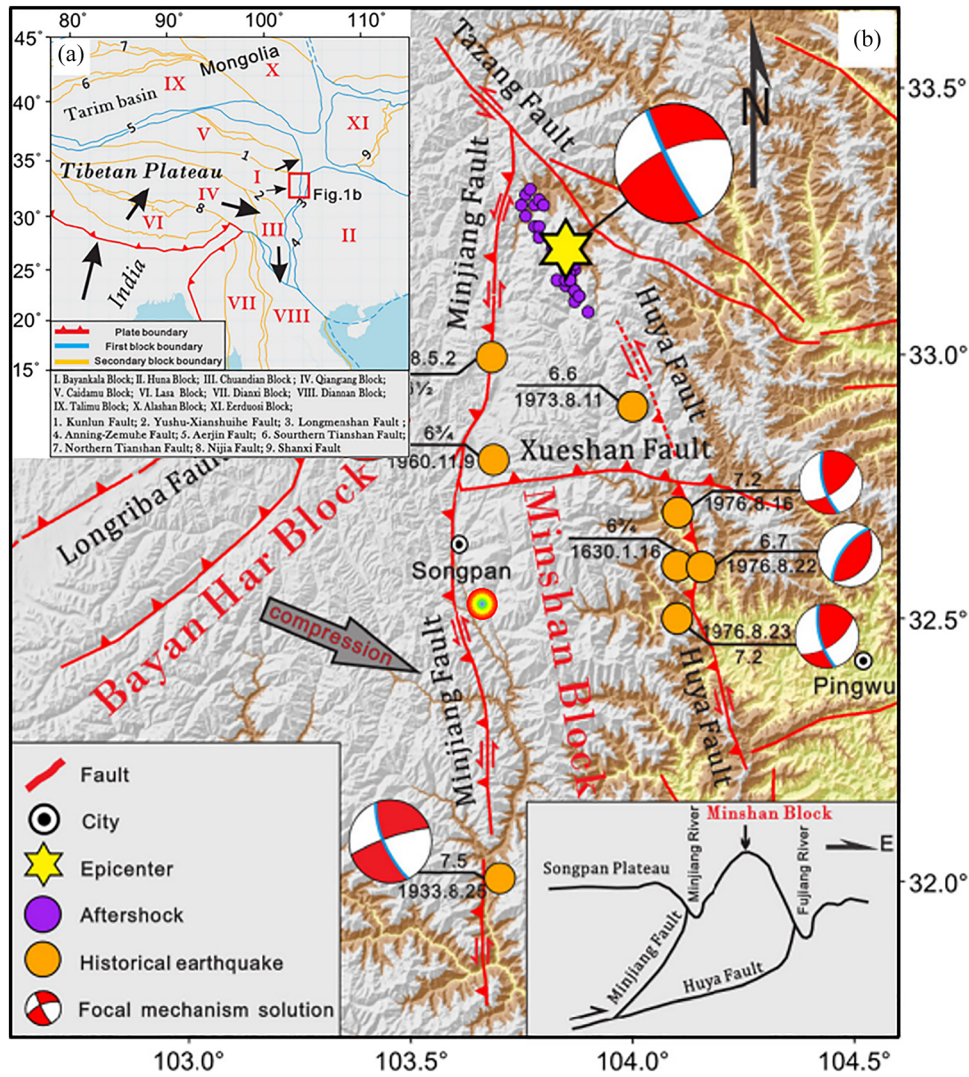


Fig. 1 Location of Minshan fault block (modified from Ref. [44])



Fig. 2 Schematic diagram of the relationship between Minjiang fault zone and tunnel line

the excavated section area reaches more than 182 m². According to the deformation severity of the tunnel, different supporting structures are adopted, as shown in Fig. 4. The

support structures mainly consist of double primary supports and secondary linings. Table 1 shows the design support parameters of the surrounding rock with severe large deformation.

2.3 Complex Rock Structure and Groundwater Conditions

The groundwater in the tunnel site is very rich. The loose and broken structure of the surrounding rock provides good channels for groundwater migration (Fig. 5a, b). For example, the water inrush of a tunnel affects the stability of adjacent rock, resulting in tunnel collapse. In addition, the underlying bedrock consists of slate, limestone, phyllite, and so on. The occurrence characteristics of the surrounding rock of the tunnel face are highly complicated (Fig. 5c, d), and the surrounding rock is severely distorted and broken.

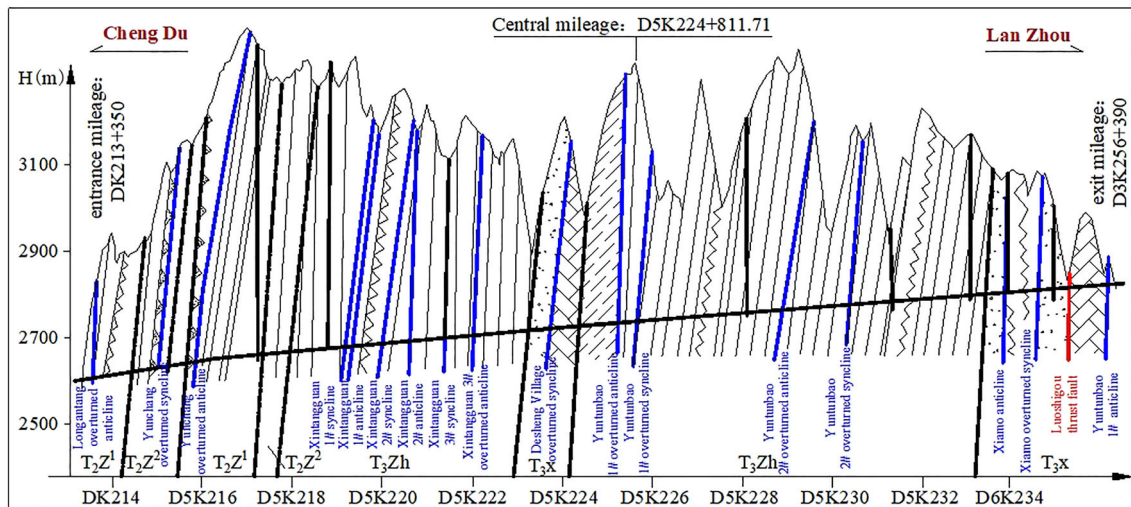


Fig. 3 The distribution of the geological structure zone during tunnelling

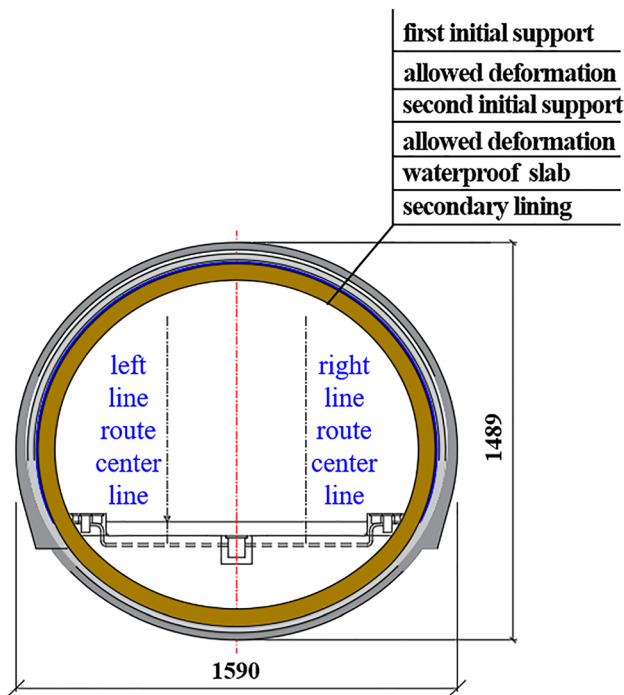


Fig. 4 Cross-section dimension of the tunnel (Unit: cm)

3 Rock Mineral Component and Mechanical Property Failure Behaviour

According to the occurrence characteristics of the surrounding rock of the tunnel face, an indoor mechanics test is first carried out to determine the mechanical behaviour of inclined and layered rock. The authors focussed on exploring the response mechanism of cyclic stress disturbances and the creep effect on the mechanical characteristics of rock during tunnelling. However, since the physical and mechanical

properties of rocks are closely related to their internal mineral composition, the rock samples are taken from the same location and same rock block and then are sealed in storage caverns. In addition, X-ray diffractometer testing should be carried out to ensure that there are no significant differences in mineral composition of the rocks.

3.1 X-Ray Diffractometer Tests

The rock mineral components are determined via X-ray diffraction. A fourth-generation multifunctional high-resolution diffractometer (Ultima series) produced by a Japanese mechanical company (Fig. 6) is used for phase qualitative and quantitative analyses. There are no special requirements for the sample size in the experiment. A small piece of stone is crushed and ground to form a powder for the measurements. The diffraction data are subsequently imported into MDI Jade 6.0 for phase identification and analysis.

As shown in Table 2, the test results reveal little difference in the types and contents of the rock mineral components. The quartz content in the rock is the highest. The second highest is carbonate minerals, i.e. calcite and dolomite, which account for approximately 30% of the total content. Clay minerals with illite content account for 15% of the total. Therefore, rocks contain approximately 45% water-sensitive minerals. The rock strength is enhanced due to the high content of quartz. However, rock strength degrades underwater due to the presence of clay minerals.

3.2 Triaxial Cyclic Loading and Unloading Test

The rock mass in underground engineering often bears persistent cumulative cyclic loading, which is the main dynamic factor of fatigue damage and deformation failure

Table 1 Supporting structures of the tunnel with severe large deformation

Main support structures	Structures types		Parameters
First layer of primary support	Sprayed concrete	Type	C30
		Thickness/cm	27
	Rock bolt	Type	Φ32
		Length/m	Tunnel crown (4 m) + sidewall (10 m) + tunnel invert (5 m)
		Spacing/m	1.2 × 0.8 (circumferential × longitudinal)
	Reinforcing mesh	Type	HPB300
		Spacing/m	0.2 × 0.2 (circumferential × longitudinal)
Steel arch	Type	HW200	
	Spacing/m	0.6	
Second layer of primary support	Sprayed concrete	Type	C30
		Thickness/cm	23
	Reinforcing mesh	Type	HPB300
		Spacing/m	0.2 × 0.2 (circumferential × longitudinal)
	Steel arch	Type	HW200
Spacing/m		0.6	
Tunnel lining	Reinforced concrete	Type	C35
		Thickness/cm	60

**Fig. 5** Underground water condition and surrounding rock structure

[48–50]. Therefore, laboratory tests include triaxial cyclic loading and unloading and triaxial cyclic loading and unloading with a static load. The test equipment includes an MTS815 multifunctional electrohydraulic servo control testing machine. Considering that the maximum tectonic stress around the tunnel site is approximately 15 MPa, the

maximum confining pressure of the indoor mechanical test is set at 15 MPa. Moreover, the confining pressure in the test process is divided into three levels: 5, 10 and 15 MPa. The conventional triaxial compression test is first carried out to determine the grading level and stress disturbance threshold of triaxial cyclic loading and unloading tests.

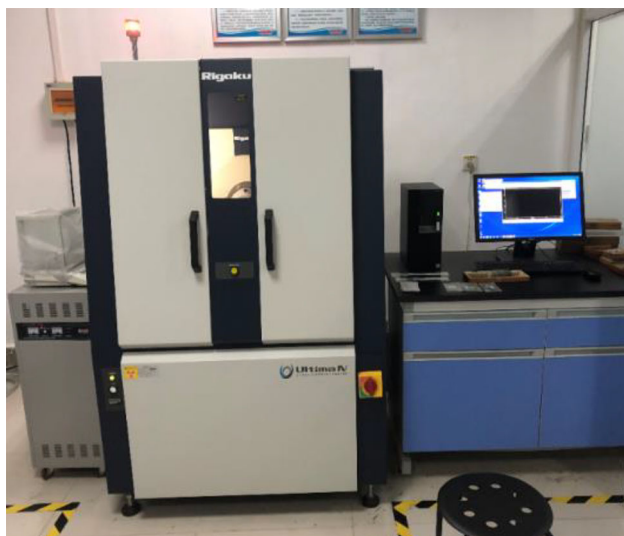


Fig. 6 X-ray diffractometer

Table 2 Mineral composition and proportion of the rock sample (%)

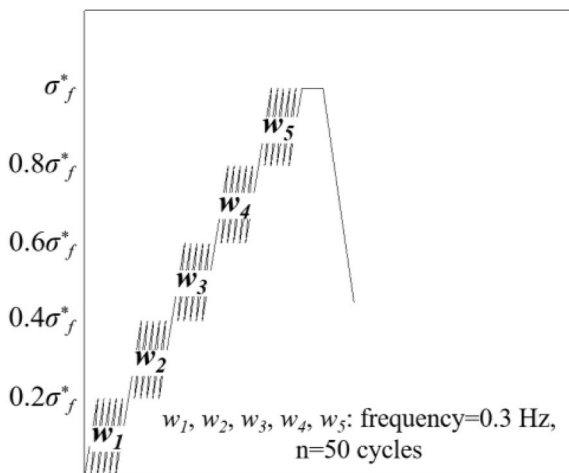
No	Test result (%)				
	Quartz	Illite	Plagioclase	Calcite	Dolomite
Rock sample 1	43	15	12	18	12
Rock sample 2	40	15	14	18	13

The axial compression takes 95% of the peak strength as the critical point. The load control (9 kN/min) is adopted before the critical point, and the controlling displacement (0.1 mm/min) is adopted after the critical point. The confining pressure of the test is controlled by the load mode (0.5 MPa/s), and the pressure was stabilised for 10 s after

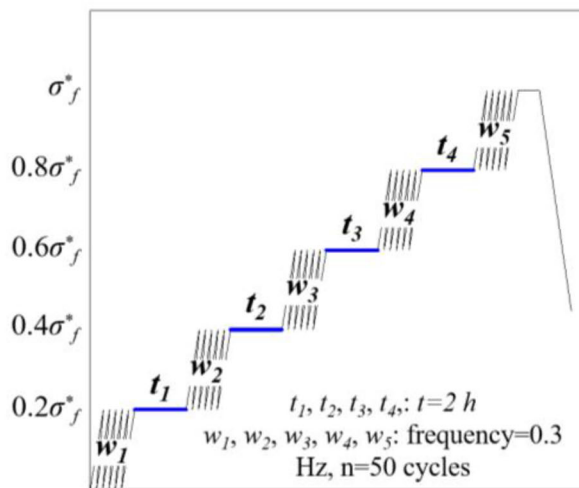
the pressure is pressed to the set value. Five loading and unloading stages are added during the cyclic loading and unloading test, as shown in Fig. 7a. The load mode is adopted in the cyclic process. From the previous cycle stage to the next cycle stage, the axial pressure increases at a rate of 9 kN/min, and the cyclic loading and unloading modes are repeated until the five stages are completed. Then the axial displacement controlling mode (0.1 mm/min) is utilised until the specimen enters the failure state. The 0.7 times the conventional triaxial peak strength (σ_f) is taken as the maximum value of the cyclic loading strength ($0.7\sigma_f = \sigma_f^*$); then the unloading points of each cycle are 0, $0.2\sigma_f^*$, $0.4\sigma_f^*$, $0.6\sigma_f^*$, $0.8\sigma_f^*$, and σ_f^* . The difference between the triaxial cyclic loading and unloading test and the triaxial cyclic loading and unloading with static load test is that after the cycle of each stage is completed, a 2 h pressure stabilisation stage is added for the latter (Fig. 7b).

Under cyclic loading, the structural plane rock samples exhibit shear failure, and there are apparent sliding scratches and powdery cuttings during the fracturing process. With low confining pressure, the deformation failure mode of the rock specimens is the combined action of tension and shear, and the rock samples break along the structural plane to form a separate thin-layered structure. However, with a high confining pressure (15 MPa), the shear fracture surface of the rock penetrates the upper and lower end faces of the rock sample, and a main shear fracture surface is regularly formed (Fig. 8a, b).

The stress–strain relationship is shown in Fig. 9, where the deformation failure of the rock samples is mainly axial. With increasing confining pressure, the brittle failure characteristics of the rock sample are weakened, and ductile characteristics appear. After five loading and unloading



(a) cyclic loading and unloading test



(b) cyclic loading and unloading with static load test

Fig. 7 Stress path of laboratory tests

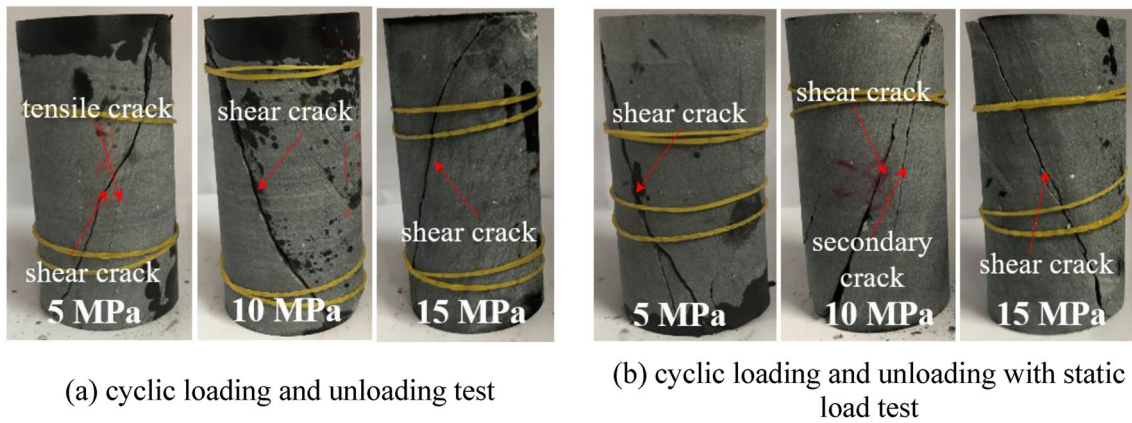


Fig. 8 Deformation failure characteristics of rock with inclined discontinuity plane

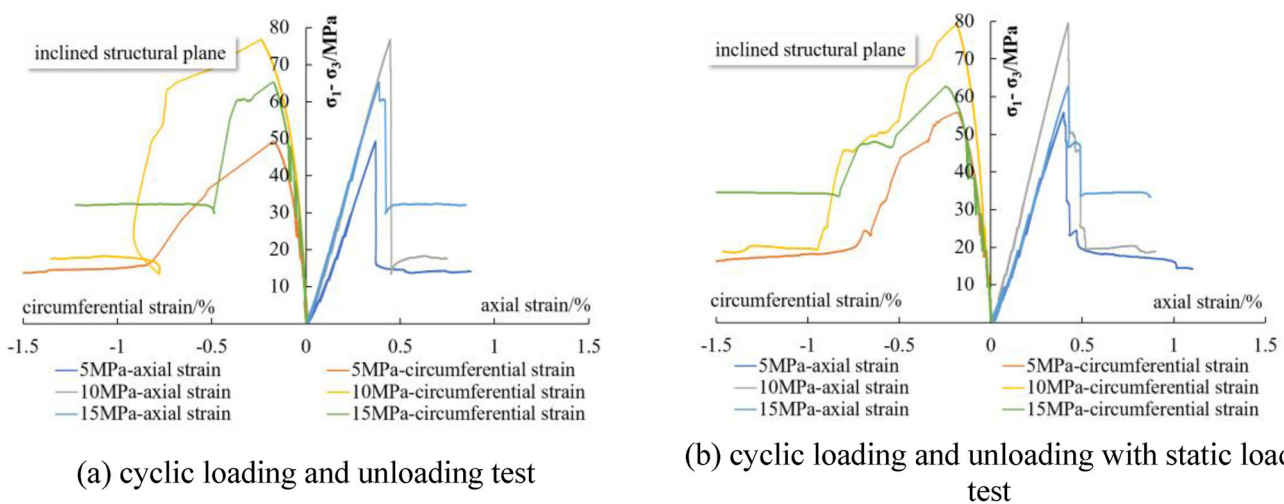


Fig. 9 Stress–strain curves of rock under cyclic loading and unloading test and different confining pressures

cycles, the stress–strain curve of the rock sample shows a stepwise growth trend, mainly related to irreversible deformation. It is a concrete reflection of the deterioration damage degree of the rock sample. In addition, due to the constraint of confining pressure, the postpeak slip deformation of the rock sample continues to increase, and the residual bearing capacity remains unchanged. This indicates that the fractured rock bound by confining pressure can continue to bear through the friction of the fracture surface. Therefore, during tunnelling, active deformation control measures such as surrounding rock grouting and rock bolt application should be adopted in a timely manner to maximise the residual bearing capacity of the broken surrounding rock close to the free face of the tunnel.

Moreover, for cyclic loading and unloading with a static load test, the stress–strain curve characteristics of the rock prepeak strength are similar to those of the cyclic loading and unloading test. However, for the stress–strain curve of the rock postpeak strength, the rock samples with inclined

structural planes exhibit a significant stepwise decrease, with an evident gradient to sudden failure characteristics. Furthermore, with increasing confining pressure, the peak strength of inclined structural plane rock under cyclic loading first increases and then decreases (Fig. 10). This phenomenon demonstrates the influence of the stress disturbance amplitude and the static load on the deformation failure of layered rock.

4 Deformation Characteristics and Mechanical Response of the Squeezing Tunnel

4.1 Tunnel Deformation Damage Characteristics

Due to the strong tectonism and complex structural characteristics of the surrounding rock, large deformation

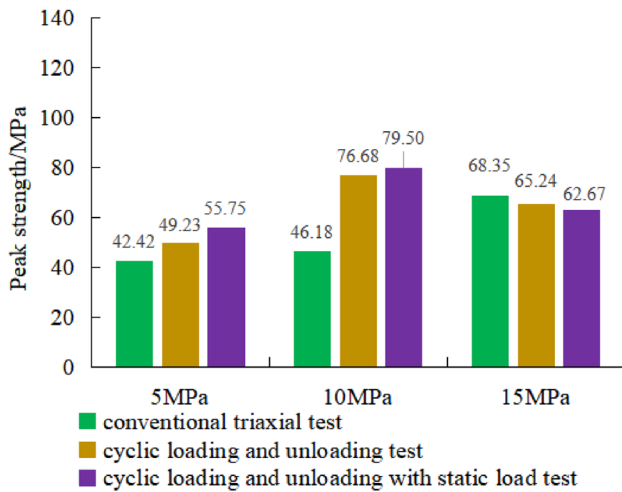


Fig. 10 Peak strength of rock under different tests

problems occur in many tunnel sections. The macroscopic deformation characteristics are as follows.

First, the significant asymmetric deformation of the surrounding rock is mainly reflected in the severe unilateral deformation of the tunnel, which leads to cracking and spalling of the shotcrete and bending and breaking of the steel arch (Fig. 11a, b). In addition, severe damage to the support structure occurs in the sidewall. Even when double-layer HW200 steel arches with higher bearing capacities are used, the primary support still experiences bending and breaking (Fig. 11c, d). Moreover, unlike the common buckling failure of steel arches along the radial direction of tunnels, steel arches also experience obvious longitudinal torsional deformation (Fig. 11e, f).

4.2 Excavation Loosening Zone Test Results

The extent of the excavation loosening zone reflects the damage degree of the surrounding rock to some extent. Moreover, the occurrence and development process of the excavation loosening zone also determine the selection of deformation control measures. In this paper, the acoustic wave method is used to test the excavation loosening zone in the field. Six groups of test boreholes are included, and the borehole depth is 20 m.

Theory and practise show that the more complete the surrounding rock is and the more concentrated the stress is, the greater the reflected wave velocity and amplitude will be. Therefore, the range of the excavation loosening zone can be determined by the changes in the reflected wave velocity and amplitude of the surrounding rock. The test process and results are shown in Fig. 12. The average range of the final excavation loosening zone is approximately 10 m, more than 60% of the designed tunnel span. This indicates that the surrounding rock has poor self-bearing capacity.

4.3 Monitoring and Analysis of the Deformation of Surrounding Rock

The construction method of the monitoring cross-section is the three-bench method, and the designed support structures are shown in Table 1. Here, laser scanning equipment and a total station are used to collect deformation data (Fig. 13). The outstanding advantage of this deformation measurement method is that it abandons the traditional total station “single point” mapping mode and can be utilised to obtain a large amount of deformation contour “point cloud” data. This

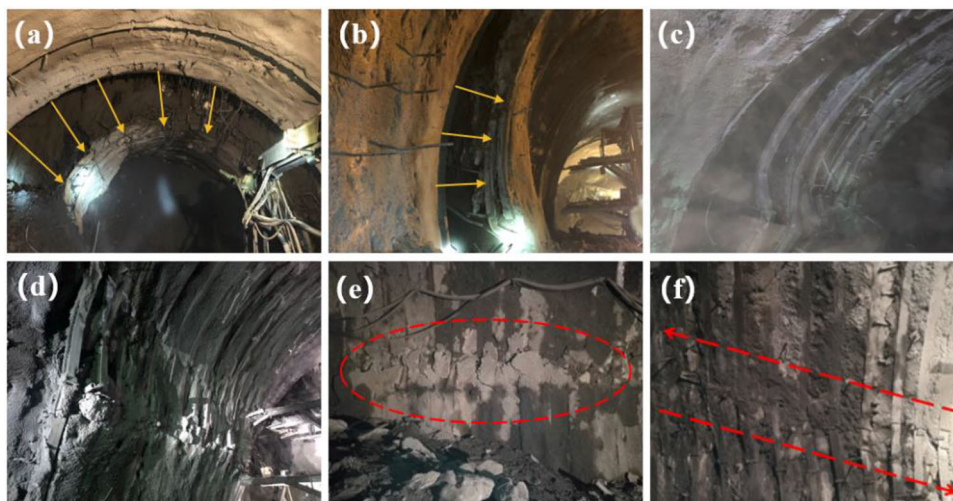


Fig. 11 Deformation failure characteristics of surrounding rock and support structures

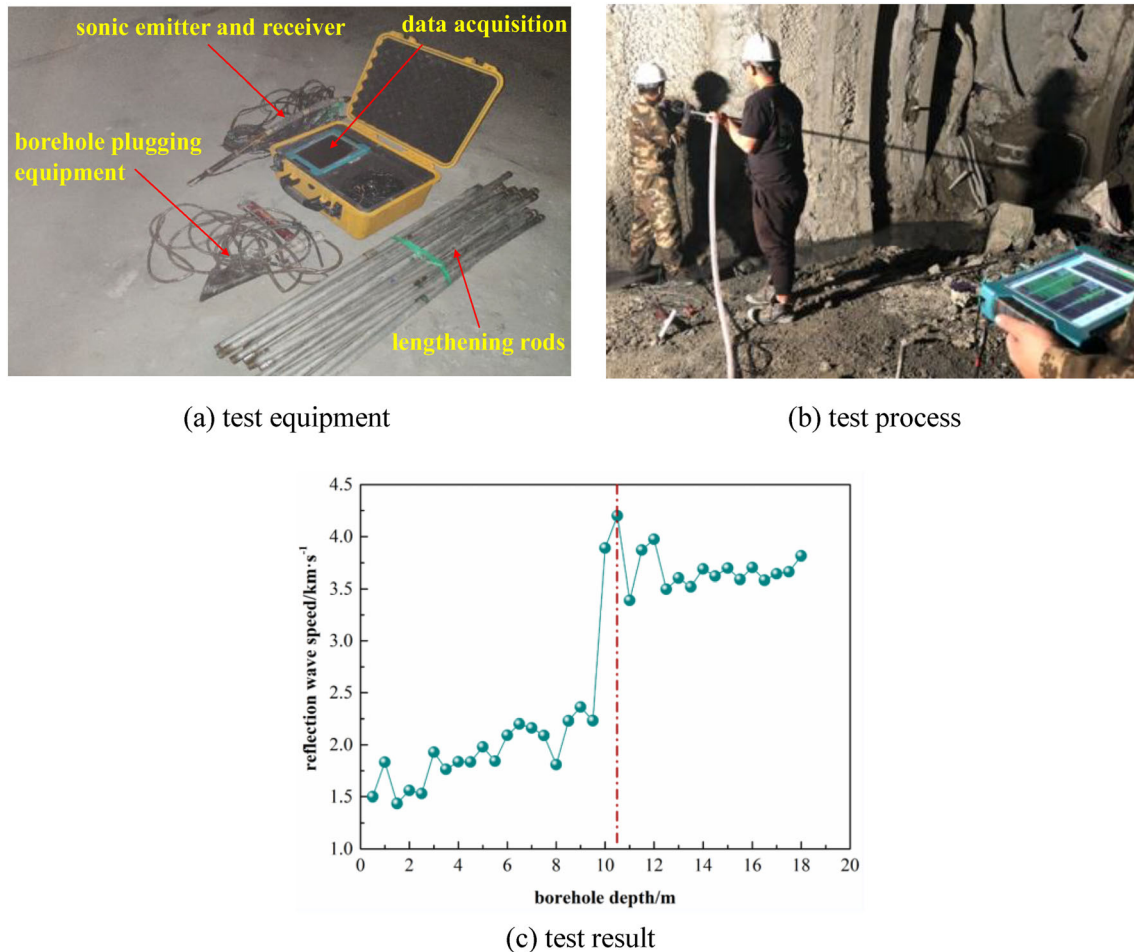


Fig. 12 Excavation loosening zone test

method can also be used to comprehensively detect tunnel overbreak, excavation volume, convergence deformation and other factors and improve the efficiency and accuracy of tunnel deformation monitoring.

As shown in Fig. 14a, the tunnel deformation shows pronounced asymmetry and is mainly horizontal convergence. The maximum settlement of the tunnel crown is approximately 1.0 m, and the maximum horizontal convergence of the upper bench can reach 2.7 m, which is approximately 2.7 times the settlement of the tunnel crown. According to the field conditions, the steel arch has been seriously bent and broken, and the shotcrete has cracked and fallen off in a large range.

In addition, the time–space effect of tunnel deformation is significant (Fig. 14b, c). According to the time-history curve of tunnel deformation, it can be divided into three stages: (1) rapid deformation development stage, which lasts approximately 20 to 25 days, from surrounding rock excavation of upper bench to second primary support implementation of upper bench; (2) slow deformation development stage, which lasts approximately 15–20 days,

from second primary support implementation of upper bench to second primary support implementation of lower bench; and (3) steady deformation development stage, which lasts approximately 20–30 days, from second primary support implementation of lower bench to the whole second primary support closure into a ring. In addition, from a spatial perspective, in the rapid deformation development stage, the distance between the monitoring cross-section and the tunnel face is usually less than 15 m, approximately one times the tunnel span. In the slow deformation development stage, the monitoring cross-section is approximately 25 m from the tunnel face, approximately 1.5 times the tunnel span. In the steady deformation development stage, the monitoring cross-section is approximately 25–45 m from the tunnel face, approximately 1.5–3.0 times the tunnel span.

Figure 14d shows the deformation rate characteristic curves of the surrounding rock. There are several areas with sudden changes in the deformation rate. Moreover, the change frequency and strength of the deformation rate are very high; the convergence deformation rate of the upper



(a) Focus^m laser scanning equipment



(b) monitoring process

Fig. 13 Monitoring tunnel deformation

bench can reach 12 cm/day, and there are 14 deformation cycles during tunnelling when the deformation rate of the surrounding rock exceeds 4 cm/day.

Generally, tunnel deformation is characterised by a large deformation, a high deformation rate and a long duration. The deformation of the surrounding rock deformation exhibits gradual changes to sudden changes, consistent with the postpeak deformation failure evolution of layered rock samples from laboratory tests. Furthermore, these sudden changes in the deformation rate not only accelerate the deformation of the surrounding rock but also aggravate the deformation and damage degree of the support structures.

4.4 Mechanical Response of the Tunnel Lining

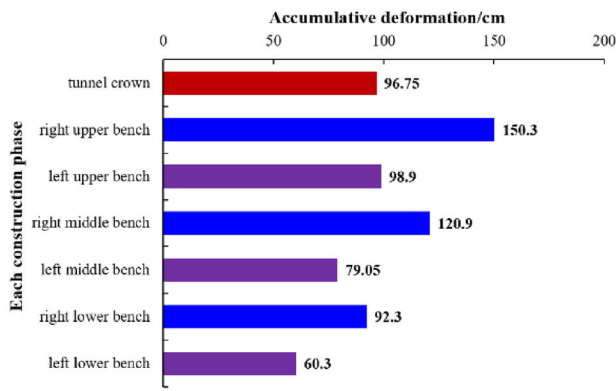
Long-term effective monitoring data of the internal force of the primary support were not obtained because the primary support was seriously damaged and because the steel arch needed to be constantly removed and replaced. Here, the stress characteristics of the tunnel lining are measured and analysed. The layout of the mechanical monitoring components of the tunnel lining is shown in Fig. 15. The pressure cell is used to monitor the contact pressure between the primary support and tunnel lining, and a reinforcement metre is used to monitor the stress state of the main reinforcement of the tunnel lining.

The evolution and time-history characteristics of the contact pressure are shown in Fig. 16a, b. During the

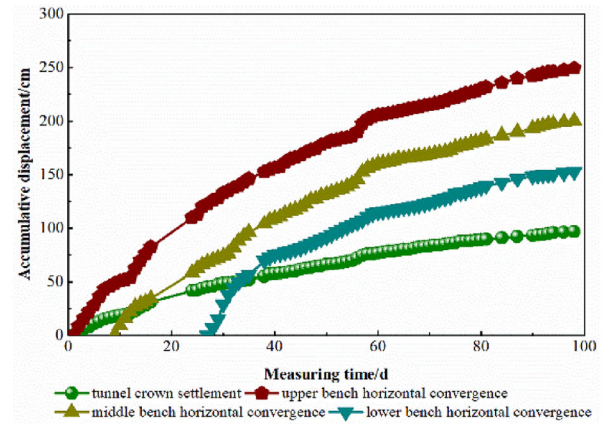
monitoring period of approximately 45 days, the contact pressure at each measuring point is high; the maximum value occurs at the left spandrel (0.73 MPa), and the minimum value occurs at the right sidewall (0.05 MPa). The phenomenon of bias stress in the tunnel lining is evident, which is adverse to the overall bearing capacity of the tunnel lining. In addition, at the initial stage of tunnel lining construction, because a stable joint bearing system is not formed with the primary support, the contact pressure fluctuates considerably, and the fluctuation lasts approximately 25 days.

The stress characteristics and time-history curve of the main steel of the tunnel lining are shown in Fig. 16c, d. The main steel at each monitoring point is under compression. The maximum stress of the main reinforcement is 144.1 MPa at the tunnel crown, and the minimum stress is 57.13 MPa at the left shoulder.

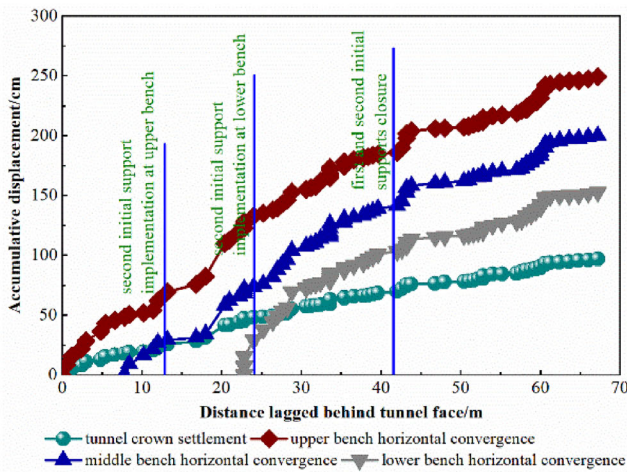
In general, in addition to the geostress, formation lithology and rock occurrence, the spatiotemporal effect of tunnel construction also significantly influences the surrounding rock deformation and force characteristics of a tunnel lining. The cyclic disturbance of tunnel excavation breaks the stress equilibrium state of the surrounding rock and leads to an apparent time effect in the development of joint fissures, deformation energy accumulation and dispersion of the surrounding rock. Moreover, the height and length of the different benches and the closing distances of the primary support during tunnelling cause tunnel deformation to have significant spatial effects.



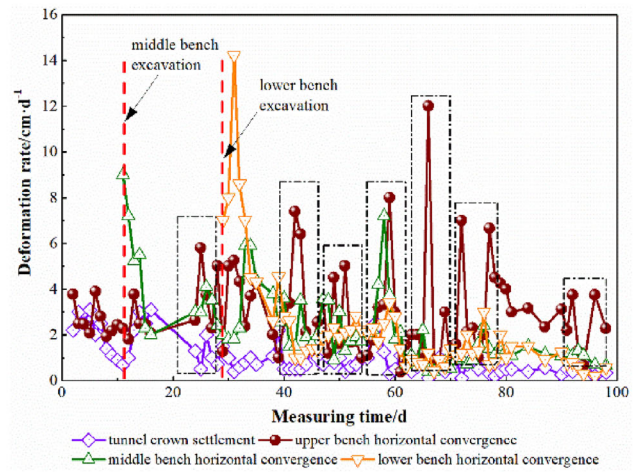
(a) accumulative deformation for each construction process



(b) time history curve of deformation characteristics

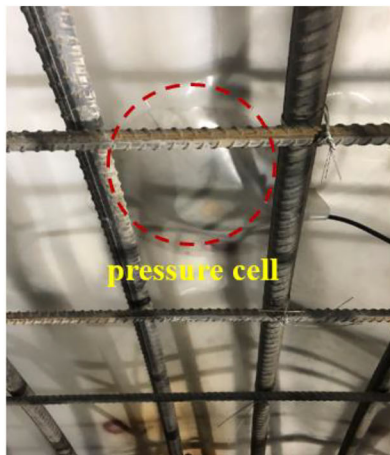


(c) space deformation characteristics

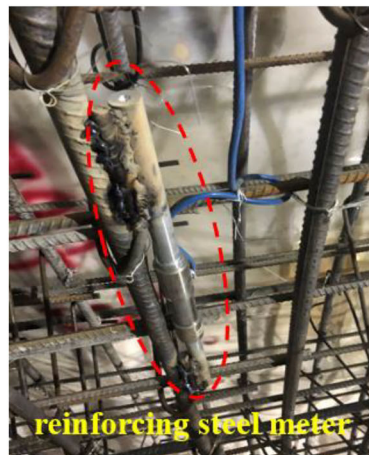


(d) deformation rate characteristics

Fig. 14 The surrounding rock deformation for each excavation step by three-bench construction method

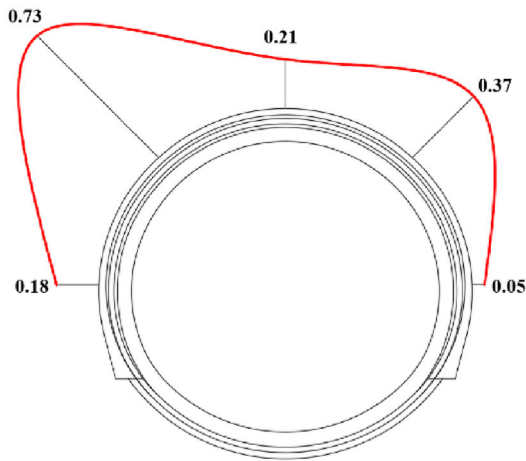


(a) pressure cell installation

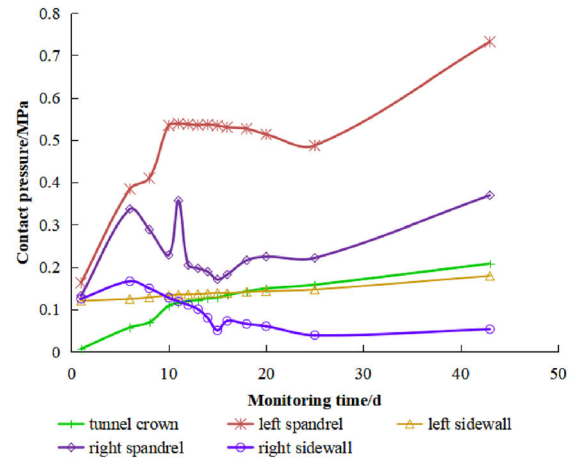


(b) reinforcing steel meter installation

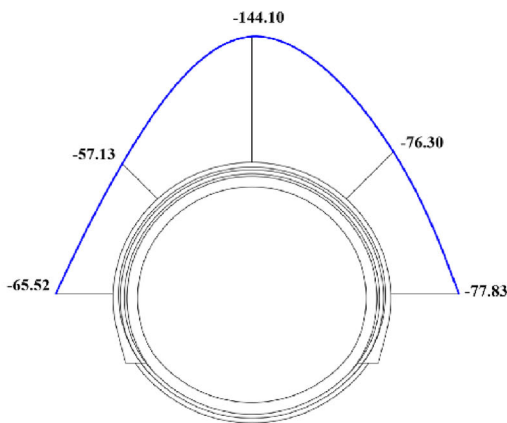
Fig. 15 Layout of mechanical monitoring components of the tunnel lining



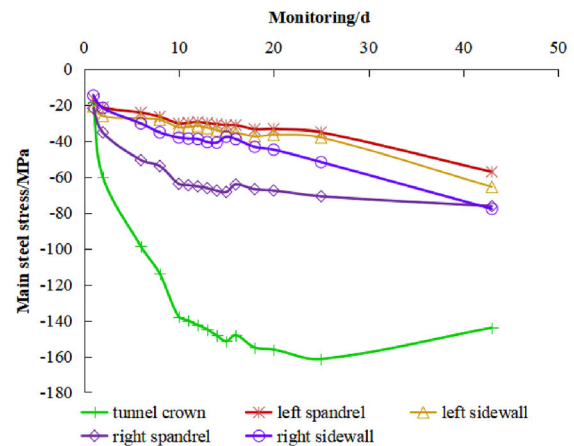
(a) envelope diagram of contact pressure



(b) time-history curve of contact pressure



(c) envelope diagram of stress of main steel



(d) time-history curve of stress of main steel

Fig. 16 Monitoring structures bearing characteristics of tunnel lining (unit: MPa)

5 Tunnel Large Deformation Control Measures and Evaluation

The deformation control measures of squeezing tunnels with inclined and layered rock in strong and active fault zones should comprehensively consider the spatiotemporal effect. First, the stress state should be improved, and the mechanical properties of the surrounding rock must be strengthened. Second, the excavation method and support structure design should be optimised to restrain and limit the local asymmetric deformation of the surrounding rock and form the deformation controlling principle of coordination of the surrounding rock and support structure deformation.

5.1 Tunnel Large Deformation Control Measures

(1) Improving the stress state of the surrounding rock:

The gradient and sudden change characteristics of the deformation failure of surrounding rock are actually the result of strong instantaneous stress adjustment. For squeezing surrounding rock, tunnel excavation breaks the stress balance and produces a high stress difference. Therefore, it is particularly important to take reasonable measures to improve the stress state of the surrounding rock and reduce its stress concentration degree. From a construction perspective, the following two steps were taken:

Unlike in conventional two-bench and three-bench excavation methods, the reserved core soil at the upper bench of the three-bench excavation method is applied during tunnelling. Due to the ability of this excavation method to minimise construction disturbance and stress differences in the surrounding rock, the construction steps are shown in Fig. 17. A detailed explanation is given as follows:

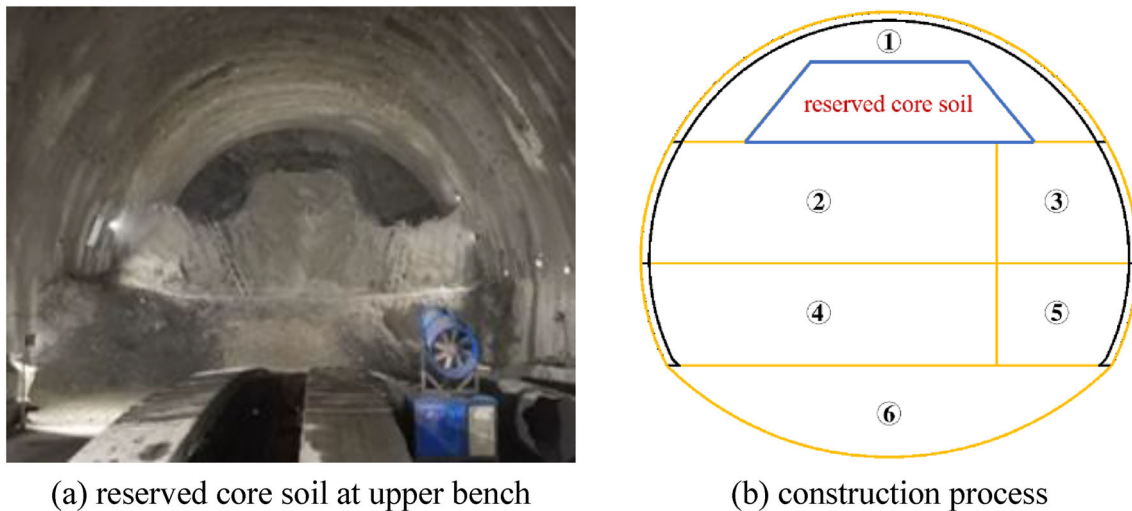


Fig. 17 Reserved core soil of upper bench of three-bench method

1. By keeping the core soil in place whilst the benches are being excavated, this method maintains a certain level of support for the surrounding rock. The reserved core soil acts as a natural support, minimising the disturbance to the surrounding rock, which in turn reduces stress differences.
2. Excavating in smaller sections allows for a more controlled readjustment of stresses in the surrounding rock. Since the surrounding rock is cut away in portions, the stress redistribution occurs incrementally, which means that at no point is there a sudden and complete release of stress that could lead to instability or failure.
3. Because the middle and lower benches do not leave the core soil, large construction machinery can conveniently operate, and support structures can also be immediately implemented to control and stabilise the deformation of the surrounding rock.

In addition, adding an advanced parallel pilot tunnel can not only improve the stress state but also reduce the internal water pressure in the surrounding rock of the main tunnel. Moreover, based on the X-ray diffraction data, the rock contains a certain amount of water-sensitive minerals. Therefore, the bearing capacity of the surrounding rock can also be enhanced eventually, and a large amount of water is released through the advance parallel pilot tunnel. The cross-section and layout of the advanced parallel pilot tunnel are shown in Fig. 18.

(2) Implementation of the long and short rock bolts:

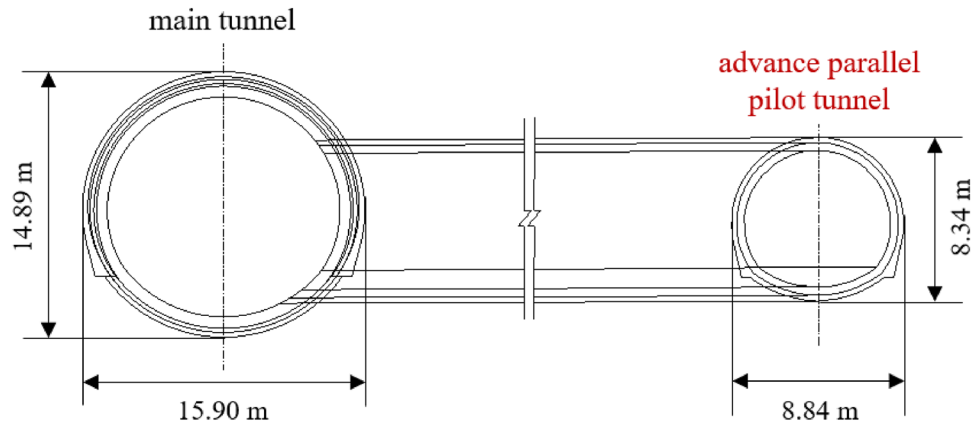
For a squeezing tunnel with steeply inclined and layered rock, the gradual and sudden change characteristics of the rock are demonstrated. That is, deformation development has a significant creep effect. In addition, similar to the deformation failure characteristics of layered rock revealed

from indoor mechanical tests, the deformation failure is mainly shear-slip along the fracture surface. Therefore, long and short rock bolts are proposed for two reasons. First, the timely implementation of short rock bolts can restrict the development of slip deformation in broken and layered rock. Moreover, long rock bolts can enhance the residual strength and bearing capacity of the surrounding rock and prevent the deformation of the surrounding rock from extending to the deep rock mass. Combined with the test results of the excavation loosening zone, it is determined that the length of the short rock bolt should not be less than 5 m and that the length of the long rock bolt should not be less than 10 m during the construction process, as shown in Fig. 19.

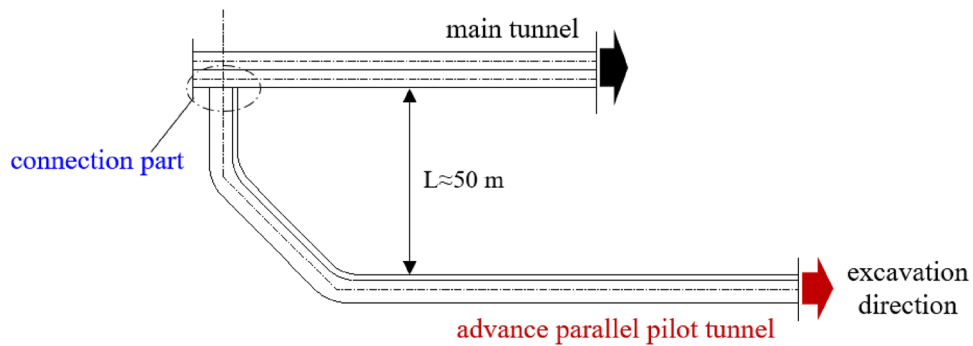
(3) Failure mechanism and strengthening measures of double primary support:

According to the deformation characteristic curve of the surrounding rock, the bearing mechanism of the double primary support is shown in Fig. 20. When relying on the first primary support, the system can only bear the deformation load $\mu_1 - \mu_0$. Then as the deformation increases, the primary support structure quickly breaks (shown in the DE curve). However, suppose that the second primary support can be followed up before the first primary support has been damaged (point D). In that case, the combined bearing capacity of the double primary support can be further exerted. The surrounding rock pressure is released (the surrounding rock pressure drops from P1 to P2), whilst the surrounding rock deformation can be controlled within μ_2 .

However, the interaction mechanism between the surrounding rock and double primary supports is very complex. First, with increasing surrounding rock deformation, the first primary support transfers the radial compressive load and shear effect to the second primary support. Suppose that the shotcrete bonding layer between the first and



(a) cross-section profile



(b) longitudinal profile

Fig. 18 Layout of advanced parallel pilot tunnel and main tunnel

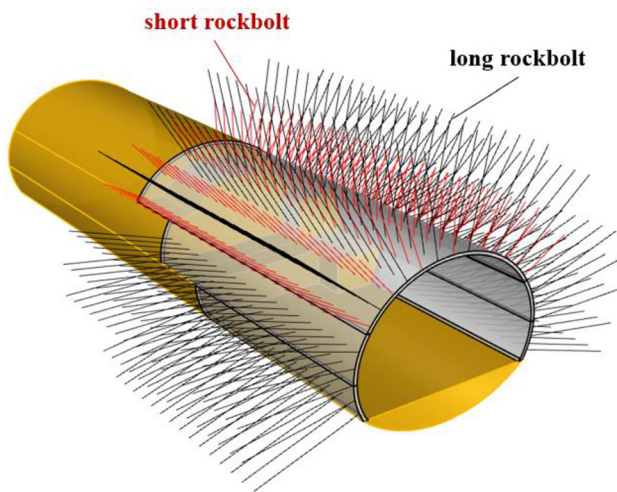


Fig. 19 Schematic diagram of implementing short and long rock bolt

the second primary support is insufficient to resist shear failure, which leads to the separation of the double primary support structure into a relatively independent bearing structure. Compared with the ideal combined bearing structure, the bearing capacity of the proposed structure is unsatisfactory. In addition, it is difficult to determine the construction timing of the second primary support. If the interval between the first and the second primary support is too short, then the whole bearing capacity of the primary support structure seems to increase. The surrounding rock pressure has not yet been effectively released, which also causes severe damage to the double support structures. If the interval time between the double primary supports is longer, then the surrounding rock load is reasonably released. However, the best construction timing for the second primary support may be missed (point D in Fig. 20), and the first primary support has entered the stage of residual bearing capacity. Eventually, the formation of a coordinated bearing system for double primary supports is problematic, resulting in a poor deformation control effect.

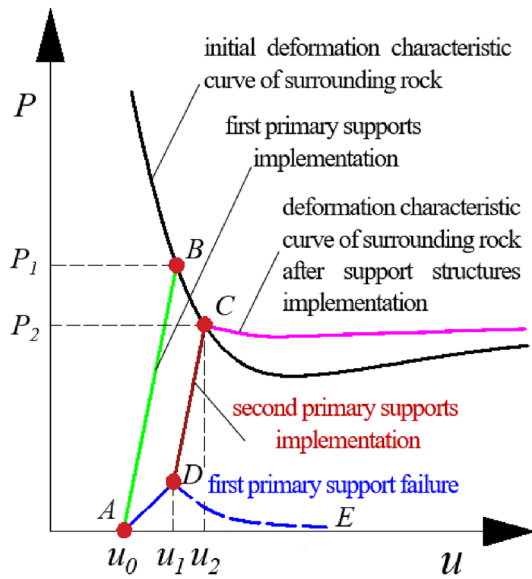


Fig. 20 Deformation characteristic curve of surrounding rock by implemented double primary support

As shown in Fig. 21, during tunnelling, the connection plates and lock-foot rock bolts of the steel arch are the weak links of deformation damage to the primary support structure. The steel arch of the double primary supports that were implemented mainly presented differential convergence deformation in the radial direction and uneven settlement in the circumferential direction. The uncoordinated deformation of the surrounding rock leads to severe local bending of the steel arch, shotcrete spalling, and other damage phenomena.

Based on the analysis of the failure mechanism of the double primary support, the following two targeted reinforcement measures are proposed:

First, a ribbed steel bar or section steel is used to lap the steel arch (Fig. 22) longitudinally to improve the anti-deformation ability and overall stability of the steel arch. Second, for the uncoordinated settlement deformation of the steel arch, a large lock-foot anchor pipe (Fig. 23) is added based on the original design of the conventional lock-foot structure. The large lock-foot structure, the $\Phi 89$



(a) crushing failure of double primary support



(b) torsion failure of double primary support

Fig. 21 Typical failure characteristics of double primary support

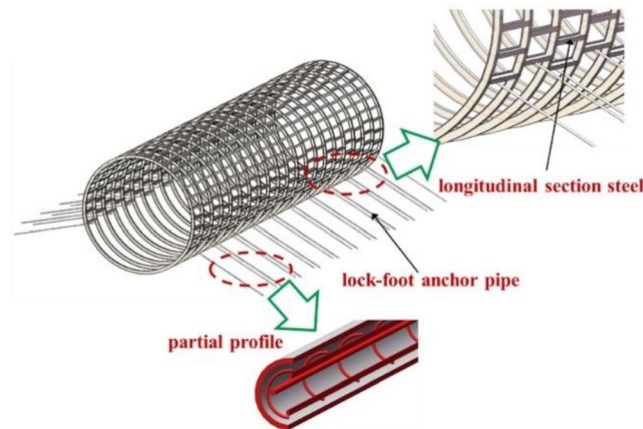


(a) steel arches connected by ribbed steel bar



(b) steel arches connected by ribbed section steel

Fig. 22 Improving longitudinal stability of steel arch



(a) position of large lock-foot anchor pipe



(b) field layout of large lock-foot anchor pipe



(c) cement slurry pouring into large lock-foot anchor pipe

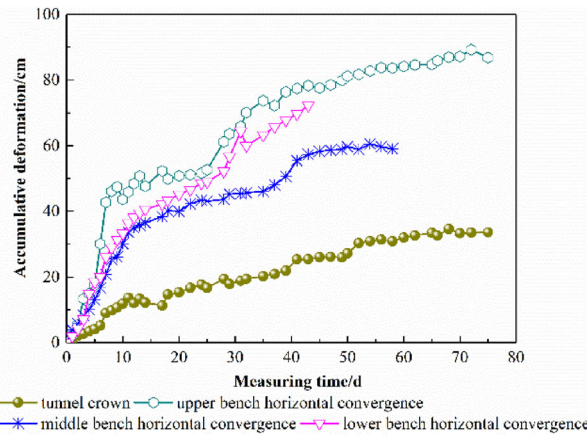
Fig. 23 The structure characteristics of large lock-foot anchor pipe

steel pipe with a wall thickness of 6 mm, is arranged between two steel arches. The length of the large lock-foot anchor pipe is 9 m. At the same time, to improve its bearing capacity and bending resistance, a four-leg hoop reinforcement cage is laid in the anchor pipe, and cement slurry is poured into the anchor pipe. In addition, the radial convergence deformation of the steel arch can also be restrained because of the bonding force and friction action between the large lock-foot anchor pipe and the surrounding rock.

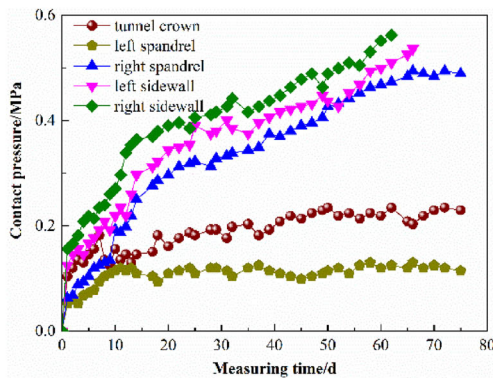
5.2 Evaluation of Construction Measures

By adopting the above deformation control measures, the tunnel deformation and structural stress state are

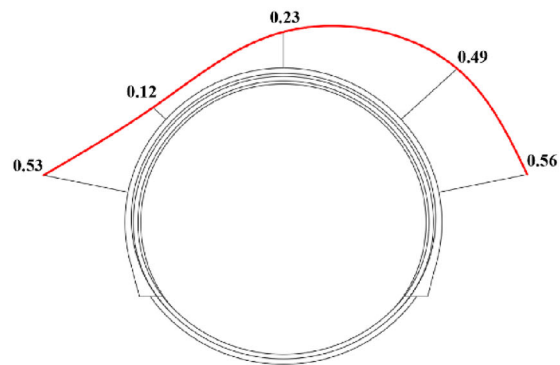
determined, as shown in Fig. 24. Although the deformation rate of the surrounding rock is rapid at the initial stage during tunnelling, the deformation development duration tends to be stable at approximately 60 days. The maximum horizontal convergence deformation is approximately 90 cm, and the maximum vault settlement deformation is 35 cm. Compared with the maximum deformation of the surrounding rock before adopting control measures, the deformation of the surrounding rock after taking these measures is significantly lower. According to the contact pressure between the surrounding rock and support structure, the structural stress fluctuates slightly at the beginning and then gradually enters a stable state. The maximum contact pressure between the surrounding rock and primary support structure is approximately 0.56 MPa at the right



(a) time-history curve of surrounding rock deformation



(b) time-history curve of contact pressure between primary support and surrounding rock



(c) maximum contact pressure between primary support and surrounding rock (MPa)

Fig. 24 Surrounding rock deformation and support structures loading of tunnel by implementing comprehensive controlling measures

haunch of the tunnel, and the minimum contact pressure between the surrounding rock and primary support structure is approximately 0.12 MPa at the left spandrel of the tunnel. Generally, by applying deformation controlling measures, the tunnel deformation is effectively controlled, the damage degree of the support structures is clearly alleviated, and sound field application results are eventually achieved.

6 Conclusion

This paper takes the steeply inclined and layered surrounding rock tunnel in a strong and active fault zone as the engineering background. Through a geological survey and laboratory and field tests, the mechanical response characteristics of layered rock and the deformation failure mechanism of support structures are analysed, and

corresponding large deformation control measures are ultimately proposed. The following conclusions can be drawn:

1. From indoor tests, the microscopic mineral composition and mechanical behaviour of inclined and layered rock are determined. The layered rock contains many water-sensitive minerals, such as carbonate and clay, at approximately 45%. Considering the creep effect and disturbance stress, the stepwise growth phenomenon of deformation before the rock reaches its prepeak strength and gradient to abrupt deformation failure characteristics after the rock reaches its postpeak strength are evaluated via triaxial cyclic and static load tests.
2. The deformation of a squeezing tunnel has significant asymmetry and nonlinearity. The maximum unilateral convergence deformation of the tunnel is large, approximately 1.5 m. In addition, gradual and sudden

changes in tunnel deformation are demonstrated, consistent with the postpeak deformation failure characteristics of layered rock in indoor tests. The range of the excavation loosening zone is approximately 10 m, reaching more than 60% of the tunnel span. The deformation rate of the surrounding rock during tunnelling is also very high, and the convergence deformation rate of the upper bench can reach 12 cm/d.

3. Due to the special structural characteristics of layered rock, the steel arch exhibits the composite failure characteristics of bending and torsion during tunnelling. Moreover, the time–space effect of tunnel deformation leads to a significant adverse effect on the tunnel lining capacity. The contact pressure values at each measuring point are very different. The maximum value is located at the left spandrel (0.73 MPa), and the minimum value is located at the right sidewall (0.05 MPa). The phenomenon of bias stress in the tunnel lining is evident, which is adverse to the overall bearing capacity of the tunnel lining.
4. The deformation control principles and corresponding technologies are summarised based on the large deformation characteristics of squeezing tunnels with inclined and layered rock. Controlling tunnel deformation should start from three aspects: adjusting the stress state of the surrounding rock, strengthening primary support structures and actively controlling deformation. Through field test verification, systematic deformation control technologies have been developed, mainly including reserved core soil at the upper bench of the three-bench method, advanced parallel pilot tunnels, long and short combined rock bolts, steel arches connected by longitudinal section steel and large lock-foot anchor pipes. Compared with the tunnel deformation before taking measures, the maximum convergence deformation is reduced from 2.7 to 0.9 m, and the bearing force of the primary support is also reasonable and stable.

Acknowledgements This work was supported by the National Natural Science Foundation of China under Grant No. 51978041.

Declarations

Conflict of Interest The authors declare that they have no conflicts of interest.

References

1. Meng LB, Li TB, Jiang Y, Wang R, Li YR (2013) Characteristics and mechanisms of large deformation in the zhegu mountain tunnel on the sichuan-tibet highway. *Tunn Undergr Space Technol* 37:157–164. <https://doi.org/10.1016/j.tust.2013.03.009>
2. Zhu HH, Yan JX, Liang WH (2019) Challenges and development prospects of ultra-long and ultra-deep mountain tunnels. *Engineering* 5(03):76–95. <https://doi.org/10.1016/j.eng.2019.04.009>
3. Tao ZG, Ren SL, Li G, Xu HT, Luo SL, He MC (2021) Model test on support scheme for carbonaceous slate tunnel in high geostress zone at high depth. *J Mt Sci* 18(3):764–778. <https://doi.org/10.1007/s11629-020-6509-1>
4. Tan ZS, Li ST, Yang Y, Wang JJ (2022) Large deformation characteristics and controlling measures of steeply inclined and layered soft rock of tunnels in plate suture zones. *Eng Fail Anal* 131:105831. <https://doi.org/10.1016/j.engfailanal.2021.105831>
5. Hoek E, Guevara R (2009) Overcoming squeezing in the Yacambú-Quibor Tunnel, Venezuela. *Rock Mech Rock Eng* 42:389–418. <https://doi.org/10.1007/s00603-009-0175-5>
6. Zhou ZH, Chen ZQ, He C, Kou H (2021) Investigation on the evolution characteristics and transfer mechanism of surrounding rock pressure for a hard-rock tunnel under high geo-stress: case study on the Erlang Mountain Tunnel, China. *Bull Eng Geol Env* 80:8339–8361. <https://doi.org/10.1007/s10064-021-02439-4>
7. Bian K, Liu J, Liu ZP, Liu SG, Ai F, Zheng XQ, Ni SH, Zhang W (2019) Mechanisms of large deformation in soft rock tunnels: a case study of Huangjiazhai Tunnel. *Bull Eng Geol Environ* 78:431–444. <https://doi.org/10.1007/s10064-017-1155-8>
8. Cao CY, Shi CH, Lei MF, Yang WC, Liu JW (2018) Squeezing failure of tunnels: a case study. *Tunn Undergr Space Technol* 77:188–203. <https://doi.org/10.1016/j.tust.2018.04.007>
9. Deng HS, Fu HL, Shi Y, Zhao YY, Hou WZ (2022) Countermeasures against large deformation of deep-buried soft rock tunnels in areas with high geostress: a case study. *Tunn Undergr Sp Tech* 119:104238. <https://doi.org/10.1016/j.tust.2021.104238>
10. Tian Y, Shu XY, Tian HM, He LK, Jin Y, Huang M (2023) Effect of horizontal stress on the mesoscopic deformation and failure mechanism of layered surrounding rock masses in tunnels. *Eng Fail Anal* 148:107226. <https://doi.org/10.1016/j.engfailanal.2023.107226>
11. Li G, Sun QH, Ma FS, Guo J, Zhao HJ, Wu YF (2023) Damage evolution mechanism and deformation failure properties of a roadway in deep inclined rock strata. *Eng Fail Anal* 143:106820. <https://doi.org/10.1016/j.engfailanal.2022.106820>
12. Man JH, Zhou ML, Zhang DM, Huang HW, Chen JY (2022) Face stability analysis of circular tunnels in layered rock masses using the upper bound theorem. *J Rock Mech Geotech Eng* 14(6):1836–1871. <https://doi.org/10.1016/j.jrmge.2021.12.023>
13. Zhou YY, Xu DP, Gu GK, Liu K, Wan LP, Wang TL, Yang JB (2019) The failure mechanism and construction practice of large underground caverns in steeply dipping layered rock masses. *Eng Geol* 250:45–64. <https://doi.org/10.1016/j.enggeo.2019.01.006>
14. Liu XZ, Liu F, Song KZ (2022) Mechanism analysis of tunnel collapse in a soft-hard interbedded surrounding rock mass: a case study of the Yangshan Tunnel in China. *Eng Fail Anal* 138:106304. <https://doi.org/10.1016/j.engfailanal.2022.106304>
15. Lu J, Yin GZ, Zhang DM, Gao H, Li CB, Li MH (2020) True triaxial strength and failure characteristics of cubic coal and sandstone under different loading paths. *Int J Rock Mech Min Sci* 135:104439. <https://doi.org/10.1016/j.ijrmms.2020.104439>
16. Wang PT, Ma C, Liu C, Liu QR, Fu YL, Cai MF (2023) Anisotropic behavior of excavated layered rock mass subjected to compression considering the joint roughness. *Bull Eng Geol Env* 82:373. <https://doi.org/10.1007/s10064-023-03400-3>
17. Jiang HP, Jiang AN, Yang XR, Zhang FR (2022) Experimental investigation and statistical damage constitutive model on layered slate under thermal-mechanical condition. *Nat Resour Res* 31(1):443–461. <https://doi.org/10.1007/s11053-021-09974-7>
18. Xu GW, He C, Yan J, Ma GY (2019) A new transversely isotropic nonlinear creep model for layered phyllite and its

- application. *Bull Eng Geol Environ* 78:5387–5408. <https://doi.org/10.1007/s10064-019-01462-w>
19. Yang SQ, Cheng L (2011) Non-stationary and nonlinear visco-elastic shear creep model for shale. *Int J Rock Mech Sci* 48(6):1011–1020. <https://doi.org/10.1016/j.ijrmmms.2011.06.007>
 20. Moussaei N, Sharifzadeh M, Sahriar K, Khosravi MH (2019) A new classification of failure mechanisms at tunnels in stratified rock masses through physical and numerical modeling. *Tunn Undergr Space Technol* 91:1–12. <https://doi.org/10.1016/j.tust.2019.103017>
 21. Zhang L, Niu FJ, Liu MH, Ju X, Wang ZW (2022) Fracture characteristics and anisotropic strength criterion of bedded sandstone. *Front Earth Sc-Switz* 10:1–10. <https://doi.org/10.3389/feart.2022.879332>
 22. Yang TJ, Wang PY, Wang SH, Liu H, Zhang Z (2023) Experimental study on shear-seepage coupling characteristics of single fractured rock mass under cyclic loading and unloading. *Rock Mech Rock Eng* 56(3):2137–2156. <https://doi.org/10.1007/s00603-022-03125-x>
 23. Lin H, Liu JF, Yang JX, Ran LN, Ding GS, Wu ZD, LYU C, Bian Y (2022) Analysis of damage characteristics and energy evolution of salt rock under triaxial cyclic loading and unloading. *J Energy Storage* 56:106145. <https://doi.org/10.1016/j.est.2022.106145>
 24. Zhang JB, Du RH, Chen YL, Huang Z (2023) Experimental investigation of the mechanical properties and energy evolution of layered phyllite under uniaxial multilevel cyclic loading. *Rock Mech Rock Eng* 56(6):4153–4168. <https://doi.org/10.1007/s00603-023-03279-2>
 25. Peng K, Zhou JQ, Zou QL, Zhang YJ, Tan GW (2020) Deformation characteristics and failure modes of sandstones under discontinuous multi-level cyclic loads. *Powder Technol* 373:599–613. <https://doi.org/10.1016/j.powtec.2020.06.076>
 26. Hu HR, Lu YY, Xia BW, Luo YF, Peng JJ, Li Y (2022) Damage characteristics of sandstone with different crack angles subjected to true triaxial cyclic loading and unloading. *Theoret Appl Fract Mech* 121:103444. <https://doi.org/10.1016/j.tafmec.2022.103444>
 27. Hu B, Yang SQ, Xu P, Cheng JL (2019) Cyclic loading-unloading creep behavior of composite layered specimens. *Acta Geophys* 67:449–464. <https://doi.org/10.1007/s11600-019-00261-x>
 28. Zhu WC, Li SH, Li S, Niu LL (2019) Influence of dynamic disturbance on the creep of sandstone: an experimental study. *Rock Mech Rock Eng* 52:1023–1039. <https://doi.org/10.1007/s00603-018-1642-7>
 29. Tang LM, Zhao YL, Liao J, Liu Q (2020) Creep experimental study of rocks containing weak interlayer under multilevel loading and unloading cycles. *Front Earth Sci* 8:519461. <https://doi.org/10.3389/feart.2020.519461>
 30. Guan K, Zhu WC, Liu XG, Wei J, Niu LL (2020) Re-profiling of a squeezing tunnel considering the post-peak behavior of rock mass. *Int J Rock Mech Min Sci* 125:104153. <https://doi.org/10.1016/j.ijrmmms.2019.104153>
 31. Sun ZY, Zhang DL, Li MY, Guo FL (2024) Large deformation characteristics and the countermeasures of a deep-buried tunnel in layered shale under groundwater. *Tunn Undergr Space Technol* 144:105575. <https://doi.org/10.1016/j.tust.2023.105575>
 32. Li ST, Tan ZS, Yang Y (2020) Mechanical analyses and controlling measures for large deformations of inclined and laminar stratum during tunnelling. *Geotech Geol Eng* 38:3095–3112. <https://doi.org/10.1007/s10706-020-01210-y>
 33. Xu GW, He C, Wang J, Chen ZQ (2020) Study on the mechanical behavior of a secondary tunnel lining with a yielding layer in transversely isotropic rock stratum. *Rock Mech Rock Eng* 53:2957–2979. <https://doi.org/10.1007/s00603-020-02107-1>
 34. Liu WW, Chen JX, Chen LJ, Luo YB, Shi Z, Wu YF (2021) Deformation evolution and failure mechanism of monoclinic and soft-hard interbedded strata: study of muzhailing tunnel. *J Perform Constr Facil* 35(5):04021042. [https://doi.org/10.1061/\(ASCE\)CF.1943-5509.0001605](https://doi.org/10.1061/(ASCE)CF.1943-5509.0001605)
 35. Chen ZQ, He C, Ma XuGW, GY, Wang WB (2019) Supporting mechanism and mechanical behavior of a double primary support method for tunnels in broken phyllite under high geo-stress: a case study. *Bull Eng Geol Env* 78(7):5253–5267. <https://doi.org/10.1007/s10064-019-01479-1>
 36. Liu WW, Chen JX, Chen LYB, LJ, Shi Z, Wu YF (2021) Deformation behaviors and mechanical mechanisms of double primary linings for large-span tunnels in squeezing rock: a case study. *Rock Mech Rock Eng* 54:2291–2310. <https://doi.org/10.1007/s00603-021-02402-5>
 37. Zhao JP, Tan ZS, Li L, Wang XY (2023) Supporting structure failure caused by the squeezing tunnel creep and its reinforcement measure. *J Mt Sci* 20(6):1774–1789. <https://doi.org/10.1007/s11629-022-7853-0>
 38. Yang K, Yan QX, Shi ZD, Zhang C, Ma SQ (2023) Numerical study on the mechanical behavior of shotcrete lining with yielding support in large deformation tunnel. *Rock Mech Rock Eng* 56:1563–1584. <https://doi.org/10.1007/s00603-022-03126-w>
 39. Petrarola DN, Plükelmann S, Mark P, Breitenbücher R (2024) Tunnel lining segments with enhanced bearing capacity using hybrid concrete concepts. *Tunn Undergr Space Technol* 143:105484. <https://doi.org/10.1016/j.tust.2023.105484>
 40. Zhou P, Jiang YF, Zhou FC, Gong L, Qiu WG, Yu JW (2022) Stability evaluation method and support structure optimization of weak and fractured slate tunnel. *Rock Mech Rock Eng* 55:6425–6444. <https://doi.org/10.1007/s00603-022-02974-w>
 41. Tao ZG, Zhao F, Wang HJ, Zhang HJ, Peng YY (2017) Innovative constant resistance large deformation bolt for rock support in high stressed rock mass. *Arab J Geosci* 10:341. <https://doi.org/10.1007/s12517-017-3127-5>
 42. Zhang JP, Liu LM, Liu CX, Li Y (2022) Mechanism and application of new prestressed yield bolt for controlling deep high-stress rock mass. *Tunn Undergr Space Technol* 119:104254. <https://doi.org/10.1016/j.tust.2021.104254>
 43. Sun XM, Zhu MQ, Zhang Y, Zhao CW, Miao CY, Zhang SK (2022) Highly prestressed NPR cable coupling support technology and its application in the deep roadway. *Eng Fail Anal* 142:106707. <https://doi.org/10.1016/j.engfailanal.2022.106707>
 44. LI Q, Tan K, Wang DZ, Zhao B, Zhang R, Li Y, Qi YJ (2018) Joint inversion of GNSS and teleseismic data for the rupture process of the 2017 Mw6.5 Jiuzhaigou, China, earthquake. *J Seismol* 22(3): 805–814. <https://doi.org/10.1007/s10950-018-9733-1>
 45. Xu X, Gao R, Guo XY, Li WH, Li HQ, Wang HY, Huang XF (2017) Outlining tectonic inheritance and construction of the Min Shan region, eastern Tibet, using crustal geometry. *Sci Rep* 7(1):13798. <https://doi.org/10.1038/s41598-017-14354-4>
 46. Zhao DZ, Qu CY, Shan XJ, Gong WY, Zhang YF, Zhang GH (2018) InSAR and GPS derived coseismic deformation and fault model of the 2017 Ms7.0 Jiuzhaigou earthquake in the Northeast Bayanhar block. *Tectonophysics* 726:86–99. <https://doi.org/10.1016/j.tecto.2018.01.026>
 47. Zhao YC, Ye GF, Dong JE, Wei WB, Jin S (2019) Electrical Constraints on the channel flow underneath the northeastern Tibetan plateau: results of the Longriba-Minjiang magnetotelluric

- sounding profile. *J Asian Earth Sci* 170:73–83. <https://doi.org/10.1016/j.jseaes.2018.10.004>
48. Seshagiri Rao K (2020) Characterization, modelling and engineering of rocks and rockmasses. *Indian Geotech J* 50(1):1–95. <https://doi.org/10.1007/s40098-020-00414-6>
49. Chen QG, Zuo YJ, Lin JY, Chen B, Zheng LJ (2022) Numerical research on response characteristics of surrounding rock for deep layered clastic rock roadway under static and dynamic loading conditions. *Geomech Geophys Geo-Energy Geo-Resour* 8(3):91. <https://doi.org/10.1007/s40948-021-00329-3>
50. Xie HP, Lu J, Li CB, Li MH, Gao MZ (2022) Experimental study on the mechanical and failure behaviors of deep rock subjected to true triaxial stress: a review. *Int J Min Sci Technol* 32(5):915–950. <https://doi.org/10.1016/j.ijmst.2022.05.006>

Springer Nature or its licensor (e.g. a society or other partner) holds exclusive rights to this article under a publishing agreement with the author(s) or other rightsholder(s); author self-archiving of the accepted manuscript version of this article is solely governed by the terms of such publishing agreement and applicable law.